ORIGINAL PAPER

Synchrotron radiation phase-contrast X-ray CT imaging of acupuncture points

**Dongming Zhang · Xiaohui Yan · Xinyi Zhang ·
Chenglin Liu · Ruishan Dang · Tiqiao Xiao ·
Peiping Zhu**

Abstract Three-dimensional (3D) topographic structures of acupuncture points were investigated by using synchrotron radiation in-line X-ray phase contrast computerized tomography. Two acupuncture points, named Zhongji (RN3) and Zusanli (ST36), were studied. We found an accumulation of microvessels at each acupuncture point region. Images of the tissues surrounding the acupuncture points do not show such kinds of structure. This is the first time that 3D images have revealed the specific structures of acupuncture points.

Keywords Acupuncture point · Synchrotron radiation · X-ray · Phase contrast · Microvessel

D. Zhang · X. Yan · X. Zhang (✉)
Synchrotron Radiation Research Center,
State Key Laboratory of Surface Physics and Department of Physics,
Fudan University,
Shanghai 200433, China
e-mail: xy-zhang@fudan.edu.cn

C. Liu
Physics Department of Yancheng Teachers' College,
Yancheng 224002, China

R. Dang
The Second Military Medical University,
Shanghai 200433, China

T. Xiao
Shanghai Synchrotron Radiation Facility,
Shanghai Institute of Applied Physics,
Chinese Academy of Sciences,
Shanghai 201800, China

P. Zhu
Beijing Synchrotron Radiation Facility,
Institute of High Energy Physics, Chinese Academy of Sciences,
Beijing 100039, China

Introduction

Acupuncture has been applied all over the world for several thousand years. Nevertheless, the mechanism of acupuncture is still not well known. Even the structure and the composition of these acupuncture points remain uncertain. In recent years, many researchers have tried to probe the basic structure of acupuncture points and to investigate the physiological mechanism of acupuncture by different methods. Some valuable discoveries have been made. For example, two visible light emission bands on the surface of acupuncture points were recorded [1]. The gathering of some trace elements (Ca, Fe, Cu, and Zn) in acupuncture points was found by the X-ray fluorescence technique [2]. Other researchers think that acupuncture points could be associated with fascial planes of connective tissue between muscles [3, 4]. Despite considerable efforts devoted to probing the anatomy of acupuncture points, however, the characterization of structures of acupuncture points is still elusive. In this report, we study the characteristic of acupuncture points by using synchrotron X-ray three-dimensional (3D) imaging to find the structural differences between acupuncture points and the surrounding tissues.

X-ray phase contrast imaging (XPCI), which uses the phase shift rather than the absorption as the imaging signal, provides the potential for substantially increased contrast when it is used on biological samples [5, 6]. By calculating the X-ray phase shift and absorption at the atomic level, XPCI was estimated to be more sensitive to light elements than the absorption-contrast X-ray imaging. Furthermore, by using XPCI together with micro-computed tomography (CT), the X-ray phase contrast computerized tomography (XPCT) technique was also developed. Various XPCT methods have been developed over the past decades. They can be classified into interferometric methods [7], diffraction-enhanced

imaging methods [8], grating-based phase contrast imaging methods [9], and in-line XPCT (IL-XPCT) methods [10]. In this work, IL-XPCT is mainly used. It is also known as propagation-based phase contrast CT. Because the synchrotron beam is sufficiently spatially coherent during the experiment, the setup of IL-XPCT is extremely simple and needs no adjustment except for the sample-to-detector distance.

Methods and materials

Principle of IL-XPCT and experimental setup

The principles of IL-XPCT, which were described in detail elsewhere [11], are briefly reviewed here. When parallel coherent light with wavelength λ irradiates samples perpendicularly, in accordance with Fresnel diffraction theory, the plane wave goes through the samples, and the intensity distribution of the disturbed wave at the downstream distance Z can be written as

$$I_\theta^Z(x,y) = \left| h_Z * U_\theta^Z \right|, \tag{1}$$

where the symbol * represents convolution, θ is the different IL-XPCT rotation angles, U_θ^z is the light complex amplitude distribution after the sample when the rotation angle is θ, and h_z is the Fresnel transmission factor, which can be written as

$$h_z(x,y) = [\exp(ikz)/i\lambda z] \exp\left[i\pi\left(x^2 + y^2\right)/\lambda z\right]. \tag{2}$$

By rotating samples, we collect the IL-XPCT projection data for every rotation angle θ between 0° and 180°. Then we can use the filtered back-projection method to reconstruct all IL-XPCT slices. Finally an internal structure image with edge enhancement of the sample can be obtained. Let $f(x_1, x_2, x_3)$ be the distribution function of the sample, and it can be written as

$$f(x_1, x_2, x_3) = \int_0^\pi I_\theta^Z * \varepsilon \, d\theta, \tag{3}$$
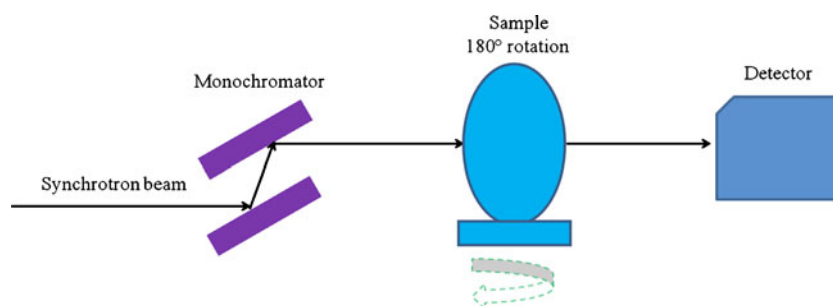
where ε is the IL-XPCT slices reconstruction filtered factor. Figure 1 shows our experimental arrangement. It consists of the specimen on a rotation stage, a monochromator, and a detector.

Sample preparation

All samples investigated were provided by the Anatomy Teaching and Research Section of the Second Military Medical University, Shanghai, China. We used New Zealand white rabbits to prepare our samples. After the adult rabbits were killed by a large dose of anesthetic, we injected 5% sodium citrate saline into the abdominal aorta for anticoagulation and to help empty the blood vessels. Then contrast agent comprising a mixed solution of barium sulfate and latex particles (their diameter is about several hundred nanometers) was injected into the abdominal aorta to make the blood vessels more highlighted in CT images. About 15 min later, samples were dissected from the rabbits and immersed in formalin for fixation.

Two acupuncture points RN3 and ST36 were studied in this work. The Chinese name of RN3 is Zhongji, and that of ST36 is Zusanli. They are frequently used in acupuncture, and the acupuncture at these points shows distinct clinical effects. Their locations are well known. RN3 is located in the abdomen at 1/13 of the distance from the pubic symphysis joint to the joint of the chest and abdomen, and ST36 is located at about 0.3 cm below the tibial tuberosity, on the dorsolateral side of the hindlimb [12, 13]. The effective diameter of these acupuncture points in rabbits is about 5 mm (should be about 10 mm for humans). Two samples were cut from RN3 and ST36 regions respectively. Each sample comprises a solid cylinder, with a height of approximately 1.2 cm and a diameter of 4.5 mm to ensure that the samples are in the acupuncture point area. The sample cut from the RN3 area is called sample A, and the sample cut from ST36 is called sample C. Samples without any acupuncture point were taken at about 3 cm away from RN3 and ST36. They are called sample B and sample D, respectively. Samples A, B, C, and D had almost the same size. All operative procedures related to animal care strictly conformed to the guidelines of the Chinese Government and the international ethical guidelines for biomedical research were also abided by in our study.
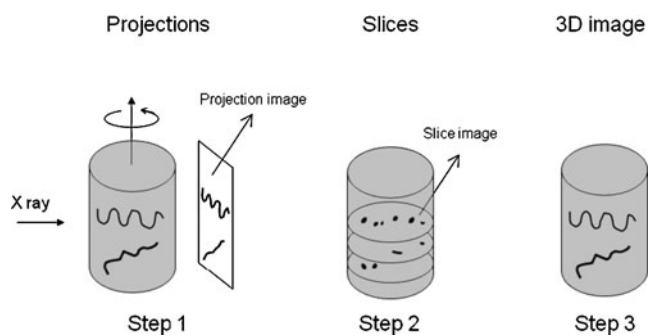

Fig. 1 Layouts of the IL-XPCT system of the BL13W experimental station, Shanghai Synchrotron Radiation Facility (SSRF)

Fig. 2 Three steps of image processing: step 1, generation of projection images; step 2, after application of a certain algorithm, slice images were obtained; and step 3, all slice images were added together to form a 3D image

Image acquisition

Experiments were performed at the 16-pole wiggler X-ray imaging and biomedical application beamline of the Shanghai Synchrotron Radiation Facility (SSRF), Shanghai, China. A monochromatic X-ray beam of 20 keV was used for the measurements. The size of the light spot on the sample was 45 (horizontal)×5 (vertical) mm^2 and the photon flux on the sample was about 5×10^{10} photons mm^{-2} s^{-1} [14]. After traversing the sample, the X-rays were recorded by a CCD camera with an effective pixel size of 9 μm. The samples were air-dried and placed in a tube filled with air, whose diameter is 4.5 mm, and then were fixed on an accurately rotatable sample stage. Rotating the sample stage around the axis of the cylinder-shaped sample, we firstly obtained the projection images, as shown in step 1 of Fig. 2, which were taken every 0.15° and we collected 1,200 images between 0° and 180°. Then after a certain algorithm, images of a number of slices (400 in this work) that were perpendicular to the axis of the sample were obtained (see step 2 in Fig. 2). The distance between two neighboring slices was about 30 μm. Finally, all slice images were added together to form a 3D image. Figure 2 shows the three steps of the transformation process from projection images to slices, and at lastly to produce a 3D image. The distance between the samples and the CCD was about 1 m and the exposure time of each image was 2 ms. For image reconstruction, a filtered back-projection algorithm was used [15]. The back noise correction, sample rotation stage axis calibration, and ring artifact correction should be applied first. Taking into account

Fig. 3 XPCI images of **a** sample A and **c** sample C, and corresponding non-acupuncture point regions from **b** sample B and **d** sample D
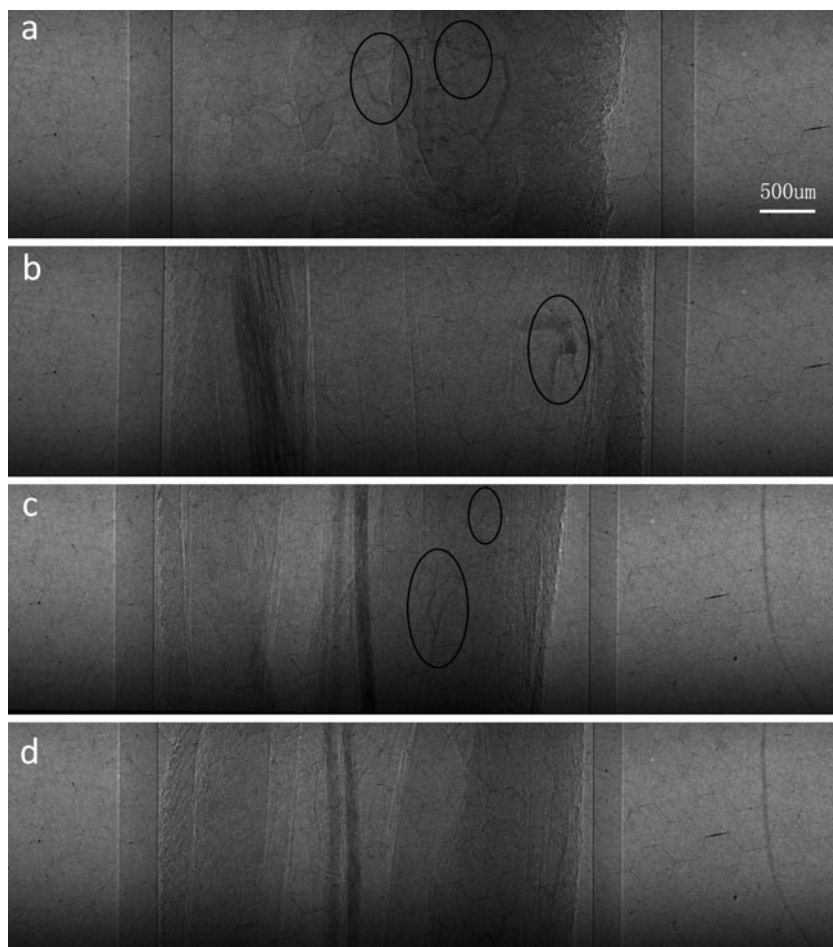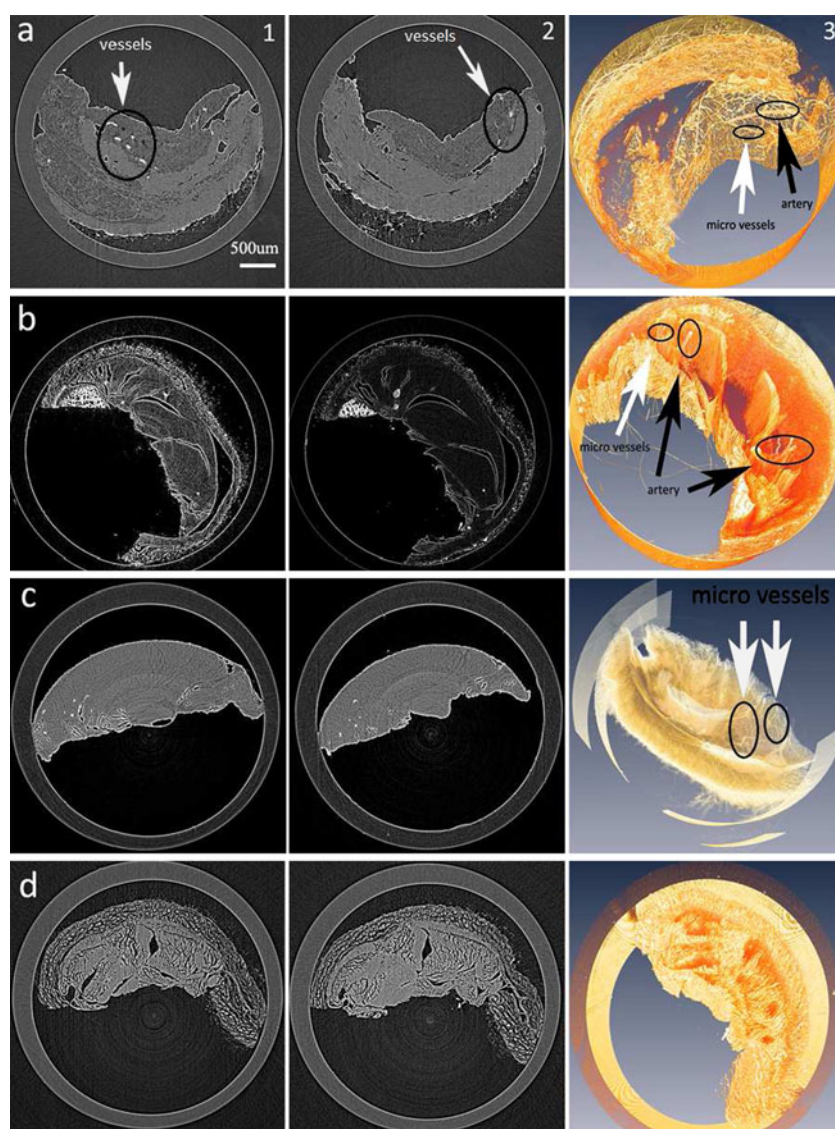
Fig. 4 IL-XPCT results of acupuncture point regions and the surrounding tissues with spatial resolution of about 15 μm for **a** RN3 acupuncture point region, **b** away from RN3 surrounding tissues, **c** ST36 acupuncture point region, and **d** away from ST36 surrounding tissues. The *first* and *second columns* are reconstructed slice images of the 102th slice and the 398th slice, respectively. The *third column* shows the 3D renderings of the samples A, B, C, and D. These 3D images were viewed along the axis perpendicular to the surface of a cylinder-like sample

Results and discussion

Figures 3a–d show XPCI projection images of samples A, B, C, and D respectively. A long blood vessel around with many fine branches is displayed clearly in the acupuncture points region (denoted by black circles in Figs. 3a and c). In contrast, in the surrounding tissues, apart from some apparent thick vessels, no complicated vessels with the same branches as shown in Figs. 3a and c can be seen (Figs. 3b and d). However, these projection images are the phase contrast images, on which the 3D structures of the samples overlapped onto a 2D plane. The overlapping of sample structures made it very difficult for these images to clearly show the structure details.

Figures 4a and b are images of sample A (RN3) and sample B; Figs. 4c and d are images of samples C (ST36) and D. After the X-ray tomographic reconstruction, we were able to reveal the 3D structure of acupuncture points through both the reconstructed slice images (first and second columns in Fig. 4) and 3D renderings (third column in Fig. 4). Samples A and B will be taken as examples to explain the details of each image.

both the thickness of the screen, which was about 0.17 mm, and the reconstruction algorithm used, we estimated the spatial resolution to be approximately 15 μm [16, 17].

Table 1 Aa%, Gg%, and Aa Gg% values of all samples

Samples	Aa%	Gg%	Aa Gg%
A	12.2±1.5	124.0±2.4	15.1±2.2
B	7.8±1.3	106.0±2.8	8.3±1.6
C	6.2±1.4	118.0±3.7	7.3±1.9
D	2.7±1.3	109.0±2.2	2.9±1.5

Figures 4a(1) and (2) are two of the IL-XPCT reconstruction slices of sample A and reveal some interesting findings. The first, supported by what can be seen in the tomographic image slices, is the contrast between the various tissue distributions through the differences of the tissue's absorptivity. Although such differentiation is usually impossible to observe based on X-ray 2D scans, our methods easily clarify these small density differences in the sample. The second observation, which can be seen from the comparison of two IL-XPCT reconstructed slices, is that the diameters of the blood vessels (the white dots denoted by arrows are surely the cross sections of vessels) are different and the distribution of them is irregular in these two slices, but the details are not explicit in this figure and will be discussed below.

Figures 4a(3) and b(3) show 3D renderings of the reconstructed volume data set of sample A and the non-acupuncture point sample B for comparison. Most of the structures, which cannot be seen in the slice images, are visible in the IL-XPCT images, including very thin hairs. For example, some long blood vessels surrounded by lots of fine branches in sample A can be seen (Fig. 4a(3)). The largest blood vessel, with a diameter of about 50 μm (denoted by the black arrow), is the artery. The fine branches vessels, whose diameter varies from approximately 15 to 40 μm, are the venule or the microvessels (denoted by the white arrow). But in the non-acupuncture point area (Fig. 4b(3)), there are only some big blood vessels (pointed out by the black arrows) with a few microvessels (pointed out by the white arrow).

Figures 4c and d show the 3D IL-XPCT images of another sample ST36 and corresponding compared surrounding tissues. As shown in Figs. 4a and b, similar accumulations of microvessels can be seen and their diameter also varies by several tens of microns.

In order to quantitatively determine the vascular accumulation in the acupuncture point regions and the surrounding tissues, the comparative vascular distribution area (Aa%) and comparative average gray-scalee value (Gg%) of Fig. 3 were calculated by computer image analysis. The ratio of the vascular area to acupuncture point area represents the comparative vascular distribution area, and the ratio of the vascular area average gray-scale value to acupuncture point area average gray-scale value represents the comparative average gray-scale value. Taking both Aa% and Gg% into account, we used Aa Gg% to represent the vascular density [18]. The calculated results are collected in Table 1, and the uncertainties are also given.

From Table 1, we can clearly see that both the vascular comparative distribution area (Aa%) and comparative average gray-scale value (Gg%) in the acupuncture point

areas are higher than those in the surrounding tissues, and the vascular density (Aa Gg%) is also much higher than that in the surrounding tissues, indicating that there is an accumulation of microvessels in these two acupuncture points areas.

Conclusions

In summary, 3D imaging of acupuncture points was successfully performed by using IL-XPCT with synchrotron radiation. The 3D structures of acupuncture points have been shown with a spacial resolution of about 15 μm. The accumulation of microvessels in acupuncture point regions is a clear characteristic, which cannot be seen in the surrounding tissues.

References

1. Zhang Y, Yan XH, Liu CL et al (2006) Photoluminescence of acupuncture point "Waiqiu" in human superficial fascia. J Lumin 119–120:96–99
2. Yan XH, Zhang XY, Liu CL et al (2009) Do acupuncture points exist? Phys Med Biol 54(9):N143–N150
3. Andrew CA, Min P, Jessica RS et al (2010) Electrical impedance of acupuncture meridians: the relevance of subcutaneous collagenous bands. PLoS ONE 5(7):e11907
4. Langevin HM, Yandow JA (2002) Relationship of acupuncture points and meridians to connective tissue planes. Anat Rec 269 (6):257–265
5. Fitzgerald R (2000) Phase-sensitive x-ray imaging. Phys Today 53:23–27
6. Momose A (2005) Recent advances in x-ray phase imaging. Jpn J Appl Phys 44:6355–6359
7. Mosose A (1995) Demonstration of phase-contrast X-ray computed tomography using an X-ray interferometer. Nucl Instrum Methods Phys Res A 352(3):622–628
8. Dilmanian FA, Zhong Z, Ren B et al (2000) Computed tomography of x-ray index of refraction using the diffraction enhanced imaging method. Phys Med Biol 45(4):933–946
9. Pfeiffer F, Kottler C, Bunk O, David C (2007) Hard X-ray phase tomography with low-brilliance sources. Phys Rev Lett 98: 108105
10. Raven C, Snigirev A, Snigireva I et al (1996) Phase-contrast microtomography with coherent high-energy synchrotron x rays. Appl Phys Lett 69(13):1826–1828
11. Spanne P, Raven C, Snigireva I, Snigirev A (1999) In-line holography and phase-contrast microtomography with high energy x-rays. Phys Med Biol 44:741
12. Shen XY, Wang H (1999) Acupuncture and Moxibustion. People's Medical Publishing House, Beijing, p 311 and 372

13. Zheng LY, Xu ZX, Zhen XC et al (2003) Objective detection and labeling of the common acupuncture points in rabbits Shanghai. J Acupunct Moxibustion 22(5):26–29

14. Chen RC, Xie HL, Luigi R et al (2010) Phase contrast micro-computed tomography of biological sample at SSRF. Tsinghua Sci Technol 15(1):102–107

15. Kak AC, Slaney M (1988) Principles of computerized tomographic imaging. IEEE, New York

16. Xie HL, Deng B, Du GH et al (2010) Advanced imaging technology and application of Shanghai synchrotron radiation source. Mod Phys 3:42–50

17. Shanghai Synchrotron Radiation Facility (2011) SSRF homepage. http://ssrf.sinap.ac.cn/english/. Accessed 27 Feb 2011

18. Gao CJ, Chen EY, Cai GJ (2005) X-anatomy study and computer image analysis of distribution of microvessel density in pulmonary carcinoma. Anat Clin 10(2):98–100